

# Stark-Many body localization in interacting infinite dimensional systems

Hristiana Atanasova,<sup>1</sup> André Erpenbeck,<sup>2</sup> Emanuel Gull,<sup>2</sup> Yevgeny Bar Lev,<sup>3</sup> and Guy Cohen<sup>1,4,\*</sup>

<sup>1</sup>*School of Chemistry, Tel Aviv University, Tel Aviv 6997801, Israel*

<sup>2</sup>*Department of Physics, University of Michigan, Ann Arbor, Michigan 48109, USA*

<sup>3</sup>*Department of Physics, Ben-Gurion University of the Negev, Beer-Sheva 84105, Israel*

<sup>4</sup>*The Raymond and Beverley Sackler Center for Computational Molecular and Materials Science, Tel Aviv University, Tel Aviv 6997801, Israel*

(Dated: November 16, 2023)

We study bulk particle transport in a Fermi–Hubbard model on an infinite-dimensional Bethe lattice, driven by a constant electric field. Previous numerical studies showed that one dimensional analogs of this system exhibit a breakdown of diffusion due to Stark many-body localization (Stark-MBL) at least up to time which scales exponentially with the system size. Here, we consider systems initially in a spin density wave state using a combination of numerically exact and approximate techniques. We show that for sufficiently weak electric fields, the wave’s momentum component decays exponentially with time in a way consistent with normal diffusion. By studying different wavelengths, we extract the dynamical exponent and the generalized diffusion coefficient at each field strength. Interestingly, we find a non-monotonic dependence of the dynamical exponent on the electric field. As the field increases towards a critical value proportional to the Hubbard interaction strength, transport slows down, becoming sub-diffusive. At large interaction strengths, however, transport speeds up again with increasing field, exhibiting super-diffusive characteristics when the electric field is comparable to the interaction strength. Eventually, at the large field limit, localization occurs and the current through the system is suppressed.

Isolated, interacting quantum systems with many degrees of freedom generically approach thermal equilibrium at least for local observables. One of the few exceptions to this is the breaking of ergodicity by sufficiently strong disorder, which leads to many-body localization (MBL) [1–5]. Advances in ultracold atomic experiments have enabled observation of the MBL phase, as well as the study of its dynamical properties and its response to external probes [6, 7]. Much of this work is driven by technological promise: MBL suppresses heating of periodically driven system [8–10], and may therefore be useful in the design of quantum information storage devices.

MBL manifests the stability of the *noninteracting* Anderson insulator [11] at sufficiently small interactions. Localization in noninteracting systems is, however, *not* limited to disordered systems. For example, single-particle states can be localized by a spatially uniform ac electric field, an effect known as dynamic localization [12, 13]; however, typically such localization mechanisms are unstable to the addition of interactions [14]. Conversely, numerical studies [15, 16] and cold atom experiments [17–19] have shown that—in the presence of a static and spatially uniform dc electric field—localization can exhibit a robustness to interactions. This phenomenon has been dubbed Stark-MBL. Nevertheless, recent studies have shown that localization might only persist up to a finite timescale controlled by the size of the system [20–22]. It is therefore a largely open question whether Stark-MBL persists in the thermodynamic limit (TDL).

Work on MBL is mostly focused on low-dimensional systems, partially due to the availability of powerful numerical techniques for one-dimensional systems, but also

because Anderson localization occurs only within states bounded by a mobility edge that shrinks with increasing dimension. Noninteracting Stark localization, on the other hand, can exist in parallel to the direction of the electric field at any dimension [23]. Due to methodological constraints, theoretical studies of stability with respect to interaction in dimensions higher than one have been limited to perturbative approaches [24]. Experimental study of a two-dimensional interacting Stark-MBL system suggests that the system is delocalized and sub-diffusive [17, 24].

The limit of infinite dimensions is accessible by way of the dynamical mean field theory (DMFT) [25–27]. This has enabled studies of the formation of long-lived, quasi-stationary currents in the presence of uniform electric fields [28], which in closed systems are eventually expected to decay due to heating at very long timescales [29]. The effect of weak interactions on the Bloch oscillations characterizing noninteracting Wannier–Stark physics has also been studied by such means [30].

In this Letter, we consider the nonequilibrium dynamics *directly* at the thermodynamic limit of an infinite-dimensional Hubbard model in the presence of a constant electric field. We show that transport is inconsistent with generalized diffusion for sufficiently strong electric fields, indicating a transition to a localized phase. Moreover, we find a non-monotonic dependence of the dynamical transport exponent on field strength: the system goes from diffusive behavior to subdiffusion, then exhibits a superdiffusive resonant phase before becoming fully localized at high field. We show that the superdiffusive behavior coincides with increases in the quasistatic currents flowing through the system, and argue that it is therefore

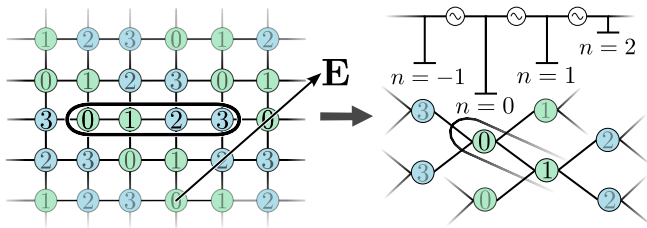


Figure 1. Model illustration. Circles represent Hubbard sites, with different colors representing different spin directions in the initial state. Lines denote hopping terms. The curved outline encompasses a unit cell, and the arrow points along the electric field. (left) 2D model with an initial condition having a periodicity of  $l = 4$ . (right) corresponding  $l = 4$  Bethe lattice with same proportions of neighboring states with each initial condition. Layers with identical electrical potential are arranged in vertical lines.

a transient nonequilibrium effect. Our results suggest that nonequilibrium physics at intermediate timescales plays an important role in many-body localization, particularly when large, high-dimensional systems are studied.

*Model.*— We investigate a particle–hole-symmetric Hubbard model describing fermions on a Bethe lattice with coordination number  $Z$ , at the limit  $Z \rightarrow \infty$ :

$$\hat{H} = -J \sum_{\langle ij \rangle \sigma} \hat{d}_{i\sigma}^\dagger \hat{d}_{j\sigma} + U \sum_i \left( \hat{n}_{i\uparrow} - \frac{1}{2} \right) \left( \hat{n}_{i\downarrow} - \frac{1}{2} \right). \quad (1)$$

Here,  $\hat{d}_{i\sigma}^{(\dagger)}$  are fermionic annihilation(creation) operators associated with lattice site  $i$  and spin  $\sigma$ , and  $\hat{n}_{i\sigma} \equiv \hat{d}_{i\sigma}^\dagger \hat{d}_{i\sigma}$ . The fermions interact through a local Coulomb repulsion of strength  $U$ , and can hop between neighboring lattice sites  $\langle ij \rangle$  with hopping amplitude  $J$ . The hopping is defined such that it is rescaled with respect to a bare hopping parameter  $t_0$ :  $J \equiv \frac{t_0}{\sqrt{Z}}$ . We set  $t_0 \equiv 1$  to be our unit of energy, and  $\hbar \equiv 1$ . As we explain below, our objective is to study generalized diffusion in this model by simulating its relaxation from periodic, nonequilibrium initial conditions characterized by discrete wavelengths; in the presence of constant, uniform electric fields applied in parallel to the waves.

We parameterize the Bethe lattices to reflect the structure of a 2D cubic lattice with the field applied along a main diagonal. The spatially homogeneous electric field enters the Hamiltonian by means of the Peierls substitution, using a pure time-dependent vector potential  $\mathbf{E}(t) = -\partial_t \mathbf{A}(t)$ . This introduces a potential difference between different diagonal layers that can be expressed as a phase in the hopping amplitudes  $t_0$ . As an initial state, except where stated otherwise, we chose the spin density wave density matrix

$$\hat{\rho}_{\mathbf{k}}(0) = \otimes_n (\sin^2(\mathbf{k}\mathbf{n}) |\uparrow\rangle \langle \uparrow| + \cos^2(\mathbf{k}\mathbf{n}) |\downarrow\rangle \langle \downarrow|)_n, \quad (2)$$

where  $\mathbf{k}$  is a wave-vector in the first Brillouin zone. We only consider  $\mathbf{k}$ 's that are parallel to the electric field (see left panel of Fig. 1), and therefore are fully defined by their wave number  $k = |\mathbf{k}|$ .

The 2D model could now be *approximately* solved within nonequilibrium DMFT [31–33], with a variety of generalizations available to provide systematic corrections [34]. Instead, we will construct an analogous infinite-dimensional model for which DMFT is *exact*, and which captures many of the relevant physical properties of the 2D system. Since the initial condition is periodic and the Hamiltonian, Eq. (1), is translationally invariant in the time-dependent gauge, it is sufficient to solve for the dynamics of  $l = \pi/k$  unique sites, which we will call a unit cell. Fig. 1 demonstrates the construction of the electric field for the Bethe lattice with infinite coordination number and same properties as the finite-dimensional model; the  $Z = 4$  version is illustrated in the right panel of Fig. 1. While one could also use, e.g., a hypercubic lattice with the field on the diagonal [27], this has a minor effect on the physics but somewhat complicates the DMFT self-consistency condition.

*Numerical solution.*— The DMFT maps the extended interacting lattice model onto a set of  $l$  effective impurity models—one for each unique site—that are coupled only by a self-consistency condition [27]. We solve the auxiliary models by three different methods of increasing complexity and precision, all of which are based on perturbative expansions in the impurity–bath hybridization. We rely mostly on the non-crossing approximation (NCA) and one-crossing approximation (OCA), which represent the lowest and next-to-lowest order self-consistent, conserving truncations in the hybridization expansion [35–43]. At shorter timescales and smaller unit cell sizes, we cross-validate results from these approximate schemes using the more computationally expensive numerically exact inchworm Quantum Monte Carlo (iQMC) method [44]. The inchworm scheme takes advantage of the causal structure of diagrammatic expansions to formulate resummed Monte Carlo methods that bypass certain sign problems, including the dynamical sign problem that usually limits nonequilibrium simulations [45–61].

*Diffusion.*— In order to analyze localization we need to understand how the initial state of the system, which is a spin density wave with wave number  $k$ , evolves in time. We assume (and later test this assumption) that in the hydrodynamic limit of  $k \rightarrow 0$  the system is well described by the fractional diffusion equation [62],

$$\frac{\partial P_n(t)}{\partial t} = D_\mu \nabla^\mu P_n(t). \quad (3)$$

Here  $P_n(t)$  is the probability to have a spin up electron on site  $n$ ,  $1 < \mu < 2$  is the dynamical exponent,  $\nabla^\mu$  is the fractional Laplacian, and  $D_\mu$  is the

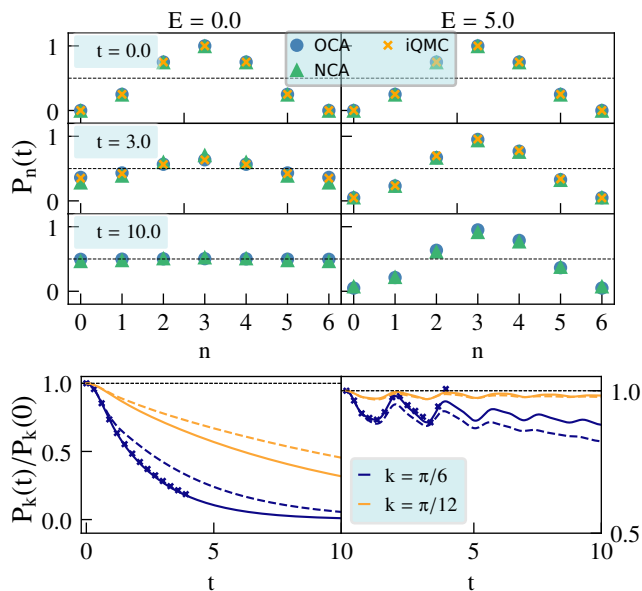


Figure 2. (upper panel) Time evolution of the spin up probability  $P_n(t)$  in equilibrium ( $E = 0$ ) and with an electric field ( $E = 5$ ) for a Coulomb interaction  $U = 2$ , with circles/triangles/crosses denoting NCA/OCA/converged iQMC results, respectively. The initial state is a spin density wave with wavenumber  $k = \pi/6$ . (lower panel) Time evolution of two Fourier components  $k = \frac{\pi}{6}, \frac{\pi}{12}$ . The dashed (solid) line denotes data obtained from NCA (OCA) calculations, while symbols represent converged iQMC results.

generalized diffusion constant. It is more convenient to work in the Fourier domain of Eq. (3),  $\frac{\partial P_k(t)}{\partial t} = -D_\mu |k|^{2\mu} P_k(t)$ , where  $P_k(t) = \sum_{n=0}^{l-1} e^{-ikn} P_n(t)$  and  $k \in \{\frac{\pi}{m} | m \in \{0, 1, \dots, l-1\}\}$ . The solution is then given by

$$P_k(t) = P_k(0) e^{-D_\mu |k|^{2\mu} t}. \quad (4)$$

This yields the following relation, which we use to extract the diffusion exponent and diffusion constant from our simulations:

$$\ln \frac{P_k(t)}{P_k(0)} = -D_\mu |k|^{2\mu} t. \quad (5)$$

We consider initial states (2), where only one  $k$ -mode is excited.

*Results.* — The upper panels of Fig. 2 show the spin up population  $P_n(t)$  at the 6 sites  $n$  within a unit cell of size  $l = 6$ , at the initial time and several later times. The initial state is a spin density wave characterized by  $k = \frac{\pi}{6}$ . Different symbols denote the two approximations and the numerically exact iQMC result, where available; this shows that the OCA is quantitatively accurate at intermediate times. In the three left panels, the electric field is turned off ( $E = 0$ ), and the spin density wave

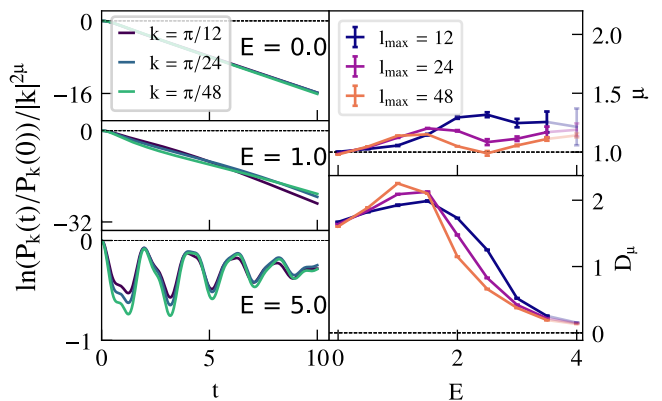


Figure 3. *Left side:* each plot shows the decay of the populations for three different initial states  $k$  scaled by  $|k|^{2\mu}$  after the diffusion coefficient  $\mu$  was estimated by fitting the data to Eq. (5). The slope of the lines is the diffusion constant  $D_\mu$ . *Right side:* dynamical exponent  $\mu$  and the generalized diffusion constant  $D_\mu$  for a system with  $U = 2$  and different maximum unit cell sizes  $l_{\max}$  used to extract  $\mu, D_\mu$  (see main text for the definition).

rapidly relaxes to a uniform equilibrium state. In the three right panels, we set the electric field to a high value ( $E = 5$ ), and the spin density wave survives to rather long times, suggesting localization.

In the lower panels of Fig. 2, we plot the Fourier transform of the spin up population,  $P_k(t)$ , as a function of time for initial states with  $k = \frac{\pi}{6}$  and  $\frac{\pi}{12}$ . Dashed and solid lines correspond to the NCA and OCA, respectively; and symbols to iQMC results, which are only evaluated for the  $k = \frac{\pi}{6}$  case. In the left panel, where  $E = 0$ , we observe a clear exponential decay for both values of  $k$ . On the right, where  $E = 5$ , we observe oscillatory dynamics that suggest eventual decay for  $k = \frac{\pi}{6}$ . For  $k = \frac{\pi}{12}$ , however, the population appears to freeze at a finite value, suggesting the onset of localization. Notably, improving the approximation by going from the NCA to the OCA enhances both trends. Furthermore, for  $k = \frac{\pi}{6}$ , comparison between the OCA and the numerically exact iQMC results shows that the OCA is accurate in this parameter regime.

If the system obeys a generalized diffusion equation, Eq. (5), curves like the ones in the bottom panels of Fig. 2 could be rescaled onto each other by plotting  $|k|^{-2\mu} \ln \frac{P_k(t)}{P_k(0)}$  as a function of time  $t$ . The left panels of Fig. 3 show how this works: for each field strength  $E$  and at a particular interaction strength  $U = 2$ , we extract the dynamical exponent  $\mu$  by fitting this single unknown parameter to minimize the minimal least square distance between curves with different  $k$ . When the relaxation is exponential, such that the physics is consistent with Eq. (5), the curves collapse onto a single, straight line. The slope of this line then uniquely determines the generalized diffusion constant  $D_\mu$ . Curiously, the curve

collapse still works even when the  $k$ -modes do not exponentially decay in time (see bottom left panel of Fig. 3 where  $E = 5$ ). In that case, however, the diffusion constant and exponent are ill-defined and we do not present them. The borderline case is plotted as slightly transparent.

Diffusion is a large wavelength phenomenon, therefore it is imperative to examine our results in the  $k \rightarrow 0$  limit; yet numerically we can only access finite values of  $l$ . In the right panels of Fig. 3 we show the dynamical exponent  $\mu$  (top) and the generalized diffusion constant  $D_\mu$  (bottom) as a function of the field  $E$  for interaction strength  $U = 2$ . Both  $\mu$  and  $D_\mu$  are computed by collapsing three sets of wave-vectors differing by the maximum unit cell size used:  $k_{l_{\max}=48} \in \{\pi/48, \pi/24, \pi/12\}$ ,  $k_{l_{\max}=24} \in \{\pi/24, \pi/12, \pi/6\}$  and  $k_{l_{\max}=12} \in \{\pi/12, \pi/6, \pi/3\}$  [63]. The set  $k_{l_{\max}=48}$  is therefore most characteristic of the hydrodynamic limit  $k \rightarrow 0$ . We see that convergence to  $k \rightarrow 0$  is obtained only at the small electric field limit, where transport is clearly diffusive ( $\mu \approx 1$ ). However, a general trend emerges at larger fields: at weak fields, transport slows down, becoming subdiffusive ( $\mu > 1$ ). This is accompanied by an increase in the diffusion constant, which then drops at higher fields. Interestingly, transport then becomes diffusive again when the electric field is of the order of the interaction strength,  $E \approx U$ . For larger electric fields transport becomes subdiffusive again and finally localizes at even higher fields. In this large  $E$  limit, Eq. (3) is no longer satisfied, and the extraction of  $\mu$  and  $D_\mu$  loses its meaning (faded symbols in Figs. 3 and 4). We note that convergence with  $l_{\max}$  is generally faster at higher  $U$  [64].

In the top two panels of Fig. 4 we plot the dynamical exponent and the generalized diffusion constant, as obtained from the result sets analogous to  $k_{l_{\max}=48}$  above, but for several values of the interaction strength  $U$ . The general trend is as in the  $U = 2$  case, but for values of  $U$  larger than 2, transport briefly becomes superdiffusive (i.e.  $\mu < 1$ ) for intermediate fields for which  $E \approx U$ . This is accompanied by a drop in the generalized diffusion constant (middle panel). The super-diffusive regime does not appear to vanish in the hydrodynamic limit,  $k \rightarrow 0$  limit (see [64]). We argue that this enhancement in transport is related to meeting the resonance condition between the field and the interaction energy of local single-charge excitations on one site. At higher fields, localization eventually sets in, preventing the interpretation as a diffusion equation (borderline cases are marked by faded symbols). At  $U = 1$ , this occurs immediately after the dip at the resonance. At higher interaction strengths, it is preceded by a second rise of  $\mu$  towards subdiffusive behavior.

To show the emergence of localization, in the bottom panel of Fig. 4 we show the current flowing through the system at the largest accessible time  $t = 10$ , after starting from a Neél state. This initial condition is chosen for

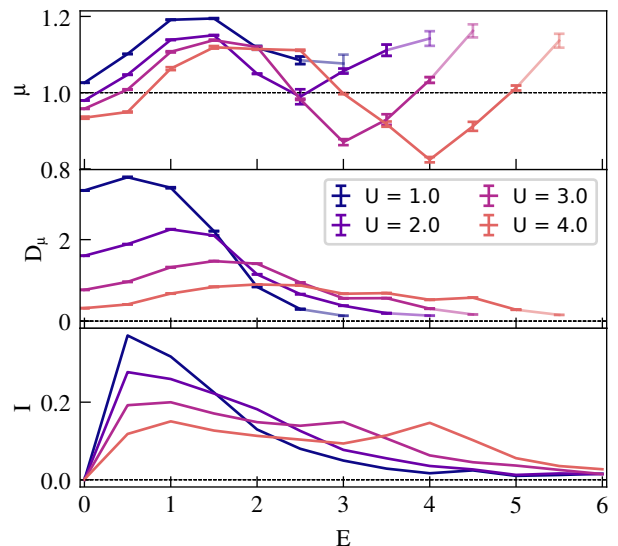


Figure 4. Dynamical exponent  $\mu$  and generalized diffusion constant  $D_\mu$  as functions of the electric field  $E$ , for various interaction strengths  $U$  and extracted from the data with minimal wave number,  $k_{l_{\max}=48}$ . The lowest panel shows the current for a system initially prepared in a Neél state at time  $t = 10$ .

numerical convenience and is not crucial here (see [64] for details). The current increases with field at small fields, then reaches a plateau and begins to decrease, before finally vanishing in the localized regime. However, at  $U = 3$  and  $U = 4$ , an increase is visible near the resonance condition, where superdiffusive exponents are observed.

*Discussion.*— Using approximate and numerically exact methods, we studied the temporal relaxation of density waves in the Hubbard model on an *infinite* Bethe lattice and in the presence of a constant electric field,  $E$ . We found that for electric fields smaller than the interaction strength, the magnitude of the waves relaxes exponentially, such that the density satisfies a fractional diffusion equation with anomalous dynamical exponent. We studied the dependence of the dynamical exponent on the interaction strength ( $U$ ) and the strength of the electric field ( $E$ ). For  $U \leq 2$ , we find sub-diffusive behavior for  $E \lesssim U$ , which crosses over to diffusion in the hydrodynamic limit ( $k \rightarrow 0$ ). For  $E \gtrsim U$  there is no visible decay of the density waves, accompanied with a vanishing current; this is consistent with a transition from a diffusive metal to an insulator. Our results suggest that the sub-diffusion, experimentally observed in a two-dimensional system [17], may result from the system being far from the hydrodynamic limit.

For  $U > 2$  the behavior is more peculiar. Here, we do not observe a significant drift of the dynamical exponent in the hydrodynamic limit. Moreover, it has a



non-monotonous dependence on the electric field  $E$ . For sufficiently small electric fields transport is diffusive with a dynamical exponent  $\mu = 1$ . Increasing the electric field makes transport sub-diffusive as long as  $E < U$ . When the electric field becomes comparable to the interaction strength, we observe a noticeable acceleration of transport all the way to super-diffusion. Further increasing the field, such that  $E \gg U$ , leads to an apparent localization. Working directly in the thermodynamic limit, our results are consistent with Refs. [20, 21], which suggest that Stark-MBL localization in a one-dimensional system is possible only in the thermodynamic limit. Regarding future work, we mainly focused on spin transport, but it would also be interesting to contrast this to density transport. Another open question is the nature of the super-diffusive transport for  $E \approx U$ , which we associated with a resonance condition between the electric field and the energy it takes to create or destroy a doublon/holon. It would be especially interesting to realize this effect in cold atoms experiments.

This research was supported by the ISRAEL SCIENCE FOUNDATION (Grants No. 2902/21, 1304/23 and No. 218/19) and by the PAZY foundation (Grant No. 318/78). Until August 31, A.E. was funded by the Deutsche Forschungsgemeinschaft (DFG, German Research Foundation) - 453644843. A.E. starting on September 1, and E.G., were supported by the U.S. Department of Energy, Office of Science, Office of Advanced Scientific Computing Research and Office of Basic Energy Sciences, Scientific Discovery through Advanced Computing (SciDAC) program under Award Number DE-SC0022088. This research used resources of the National Energy Research Scientific Computing Center, a DOE Office of Science User Facility supported by the Office of Science of the U.S. Department of Energy under Contract No. DE-AC02-05CH11231 using NERSC award BES-ERCAP0021805.

---

\* [gcohen@tau.ac.il](mailto:gcohen@tau.ac.il)

- [1] D. Basko, I. Aleiner, and B. Altshuler, *Ann Phys (N Y)* **321**, 1126 (2006).
- [2] I. V. Gornyi, A. D. Mirlin, and D. G. Polyakov, *Phys. Rev. Lett.* **95**, 206603 (2005).
- [3] R. Nandkishore and D. A. Huse, *Annu. Rev. Condens. Matter Phys.* **6**, 15 (2015).
- [4] D. A. Abanin, E. Altman, I. Bloch, and M. Serbyn, *Rev. Mod. Phys.* **91**, 021001 (2019).
- [5] F. Alet and N. Laflorencie, *C R Phys* **19**, 498 (2018).
- [6] M. Schreiber, S. S. Hodgman, P. Bordia, H. P. Lüschen, M. H. Fischer, R. Vosk, E. Altman, U. Schneider, and I. Bloch, *Science* **349**, 842 (2015).
- [7] J.-Y. Choi, S. Hild, J. Zeiher, P. Schauss, A. Rubio-Abadal, T. Yefsah, V. Khemani, D. A. Huse, I. Bloch, and C. Gross, *Science* **352**, 1547 (2016).
- [8] D. A. Abanin, W. De Roeck, and F. Huveneers, *Ann. Phys.* **372**, 1 (2016).
- [9] A. Lazarides, A. Das, and R. Moessner, *Phys. Rev. Lett.* **115**, 030402 (2015).
- [10] P. Ponte, A. Chandran, Z. Papić, and D. A. Abanin, *Annals of Physics* **353**, 196 (2015).
- [11] P. W. Anderson, *Phys. Rev.* **109**, 1492 (1958).
- [12] D. H. Dunlap and V. M. Kenkre, *Physical Review B* **34**, 3625 (1986).
- [13] D. Dunlap and V. Kenkre, *Physics Letters A* **127**, 438 (1988).
- [14] Y. Bar Lev, D. J. Luitz, A. Lazarides, Y. B. Lev, and A. Lazarides, *SciPost Physics* **3**, 029 (2017).
- [15] M. Schulz, C. A. Hooley, R. Moessner, and F. Pollmann, *Phys. Rev. Lett.* **122**, 040606 (2019).
- [16] E. van Nieuwenburg, Y. Baum, and G. Refael, *Proc. Natl. Acad. Sci.* **116**, 9269 (2019).
- [17] E. Guardado-Sanchez, A. Morningstar, B. M. Spar, P. T. Brown, D. A. Huse, and W. S. Bakr, *Physical Review X* **10**, 011042 (2020).
- [18] S. Scherg, T. Kohlert, P. Sala, F. Pollmann, B. Hebbe Madhusudhana, I. Bloch, and M. Aidelsburger, *Nat. Commun.* **12**, 4490 (2021).
- [19] W. Morong, F. Liu, P. Becker, K. S. Collins, L. Feng, A. Kyprianidis, G. Pagano, T. You, A. V. Gorshkov, and C. Monroe, *Nature* **599**, 393 (2021).
- [20] G. Zisling, D. M. Kennes, and Y. Bar Lev, *Phys. Rev. B* **105**, L140201 (2022).
- [21] B. Kloss, J. C. Halimeh, A. Lazarides, and Y. Bar Lev, *Nat. Commun.* **14**, 3778 (2023).
- [22] T. M. Gunawardana and B. Buča, *Physical Review B* **106**, L161111 (2022).
- [23] G. H. Wannier, *Phys. Rev.* **117**, 432 (1960).
- [24] P. Zhang, *Phys. Rev. Res.* **2**, 033129 (2020).
- [25] W. Metzner and D. Vollhardt, *Physical Review Letters* **62**, 324 (1989).
- [26] A. Georges and G. Kotliar, *Physical Review B* **45**, 6479 (1992).
- [27] A. Georges, G. Kotliar, W. Krauth, and M. J. Rozenberg, *Rev. Mod. Phys.* **68**, 13 (1996).
- [28] M. Eckstein, T. Oka, and P. Werner, *Physical Review Letters* **105**, 146404 (2010).
- [29] M. Mierzejewski and P. Prelovšek, *Physical Review Letters* **105**, 186405 (2010).
- [30] M. Eckstein and P. Werner, *Physical Review Letters* **107**, 186406 (2011).
- [31] J. K. Freericks, V. M. Turkowski, and V. Zlatić, *Phys. Rev. Lett.* **97**, 266408 (2006).
- [32] H. Aoki, N. Tsuji, M. Eckstein, M. Kollar, T. Oka, and P. Werner, *Rev. Mod. Phys.* **86**, 779 (2014).
- [33] V. Turkowski, “Nonequilibrium dmft,” in *Dynamical Mean-Field Theory for Strongly Correlated Materials* (Springer International Publishing, Cham, 2021) pp. 223–272.
- [34] T. A. Maier, M. Jarrell, T. Pruschke, and M. Hettler, *Reviews of Modern Physics* **77**, 1027 (2005).
- [35] N. E. Bickers, *Rev. Mod. Phys.* **59**, 845 (1987).
- [36] T. Pruschke and N. Grewe, *Zeitschrift für Physik B Condensed Matter* **74**, 439 (1989).
- [37] T. Pruschke, D. L. Cox, and M. Jarrell, *Phys. Rev. B* **47**, 3553 (1993).
- [38] K. Haule, S. Kirchner, J. Kroha, and P. Wölfle, *Phys. Rev. B* **64**, 155111 (2001).
- [39] M. Eckstein and P. Werner, *Phys. Rev. B* **82**, 115115 (2010).

- [40] R. Härtle, G. Cohen, D. R. Reichman, and A. J. Millis, *Physical Review B* **88**, 235426 (2013).
- [41] G. Cohen, D. R. Reichman, A. J. Millis, and E. Gull, *Phys. Rev. B* **89**, 115139 (2014).
- [42] A. Erpenbeck, E. Gull, and G. Cohen, *Phys. Rev. B* **103**, 125431 (2021).
- [43] A. Erpenbeck and G. Cohen, *SciPost Phys.* **10**, 142 (2021).
- [44] G. Cohen, E. Gull, D. R. Reichman, and A. J. Millis, *Phys. Rev. Lett.* **115**, 266802 (2015).
- [45] A. E. Antipov, Q. Dong, J. Kleinhenz, G. Cohen, and E. Gull, *Phys. Rev. B* **95**, 085144 (2017).
- [46] H.-T. Chen, G. Cohen, and D. R. Reichman, *J. Chem. Phys.* **146**, 054105 (2017).
- [47] H.-T. Chen, G. Cohen, and D. R. Reichman, *J. Chem. Phys.* **146**, 054106 (2017).
- [48] A. Boag, E. Gull, and G. Cohen, *Phys. Rev. B* **98**, 115152 (2018).
- [49] M. Ridley, V. N. Singh, E. Gull, and G. Cohen, *Physical Review B* **97**, 115109 (2018).
- [50] M. Ridley, E. Gull, and G. Cohen, *The Journal of Chemical Physics* **150**, 244107 (2019).
- [51] M. Ridley, M. Galperin, E. Gull, and G. Cohen, *Physical Review B* **100**, 165127 (2019).
- [52] I. Krivenko, J. Kleinhenz, G. Cohen, and E. Gull, *Physical Review B* **100**, 201104(R) (2019).
- [53] Z. Cai, J. Lu, and S. Yang, *Commun. Pure Appl. Math.* **73**, 2430 (2020).
- [54] Z. Cai, J. Lu, and S. Yang, “Numerical analysis for inchworm monte carlo method: Sign problem and error growth,” (2020), [arXiv:arXiv:2006.07654 \[math.NA\]](https://arxiv.org/abs/2006.07654).
- [55] J. Kleinhenz, I. Krivenko, G. Cohen, and E. Gull, *Physical Review B* **102**, 205138 (2020).
- [56] S. Yang, Z. Cai, and J. Lu, *New Journal of Physics* (2021), [10.1088/1367-2630/ac02e1](https://doi.org/10.1088/1367-2630/ac02e1).
- [57] Z. Cai, J. Lu, and S. Yang, *Computer Physics Communications* **278**, 108417 (2022).
- [58] J. Kleinhenz, I. Krivenko, G. Cohen, and E. Gull, *Physical Review B* **105**, 085126 (2022).
- [59] A. J. Kim, J. Li, M. Eckstein, and P. Werner, *Physical Review B* **106**, 085124 (2022).
- [60] J. Li, Y. Yu, E. Gull, and G. Cohen, *Physical Review B* **105**, 165133 (2022).
- [61] A. Erpenbeck, E. Gull, and G. Cohen, *Phys. Rev. Lett.* **130**, 186301 (2023).
- [62] R. Metzler and J. Klafter, *Physics Reports* **339**, 1 (2000).
- [63] While we could use the largest unit cell size,  $l = l_{\max}$ , to compute all three values of  $k$ , this would be computationally wasteful. Therefore we choose  $l = \pi/k$  in our computations.
- [64] See Supplemental Material at [URL will be inserted by publisher] for data allowing convergence analysis of finite size effects in obtaining transport coefficients, as well as time in obtaining the current.